Final version published as: Zhu, Y., Shan, X., Safarpour, F., Erro Go, N., Li, N., Shan, A., Huang, M. C., Deen, M., Holicek, V., Ashmus, R., Madden, Z., Gorski, S., Silverman, M. A., & Vocadlo, D. J. (2018). Pharmacological Inhibition of O-GlcNAcase Enhances Autophagy in Brain through an mTOR-Independent Pathway. ACS Chemical Neuroscience, 9(6), 1366–1379. https://doi.org/10.1021/acschemneuro.8b00015.

Pharmacological Inhibition of O-GlcNAcase Enhances Autophagy in Brain through an mTOR-Independent Pathway

Yanping Zhu,[†,‡,§] Xiaoyang Shan,[†] Farzaneh Safarpour,[§,∥] Nancy Erro Go,[⊥] Nancy Li,[‡] Alice Shan,[†] Mina C. Huang,[§,∥] Matthew Deen,[†] Viktor Holicek,[†] Roger Ashmus,[†] Zarina Madden,[†] Sharon Gorski,[‡,§,⊥] Michael A. Silverman,[§,∥] and David J. Vocadlo*[,†,‡,§]

[†]Department of Chemistry, Simon Fraser University, Burnaby, British Columbia V5A 1S6, Canada

[‡]Department of Molecular Biology and Biochemistry, Simon Fraser University, Burnaby, British Columbia V5A 1S6, Canada

[§]Centre for Cell Biology, Development, and Disease, Simon Fraser University, Burnaby, British Columbia V5A 1S6, Canada

[∥]Department of Biological Sciences, Simon Fraser University, Burnaby, British Columbia V5A 1S6, Canada

[⊥]The Genome Sciences Centre, BC Cancer Agency, Vancouver, British Columbia V5Z 1L3, Canada

ABSTRACT: The glycosylation of nucleocytoplasmic proteins with O-linked *N*-acetylglucosamine residues (O-GlcNAc) is conserved among metazoans and is particularly abundant within brain. O-GlcNAc is involved in diverse cellular processes ranging from the regulation of gene expression to stress response. Moreover, O-GlcNAc is implicated in various diseases including cancers, diabetes, cardiac dysfunction, and neurodegenerative diseases. Pharmacological inhibition of O-GlcNAcase (OGA), the sole enzyme that removes O-GlcNAc, reproducibly slows neurodegeneration in various Alzheimer's disease (AD) mouse models manifesting either tau or amyloid pathology. These data have stimulated interest in the possibility of using OGA-selective inhibitors as pharmaceuticals to alter the progression of AD. The mechanisms mediating the neuroprotective effects of OGA inhibitors, however, remain poorly understood. Here we show, using a range of methods in neuroblastoma N2a cells, in primary rat neurons, and in mouse brain, that selective OGA inhibitors stimulate autophagy through an mTOR-independent pathway without obvious toxicity. Additionally, OGA inhibition significantly decreased the levels of toxic protein species associated with AD pathogenesis in the JNPL3 tauopathy mouse model as well as the 3×Tg-AD mouse model. These results strongly suggest that OGA inhibitors act within brain through a mechanism involving enhancement of autophagy, which aids the brain in combatting the accumulation of toxic protein species. Our study supports OGA inhibition being a feasible therapeutic strategy for hindering the progression of AD and other neurodegenerative diseases. Moreover, these data suggest more targeted strategies to stimulate autophagy in an mTOR-independent manner may be found within the O-GlcNAc pathway. These findings should aid the advancement of OGA inhibitors within the clinic.

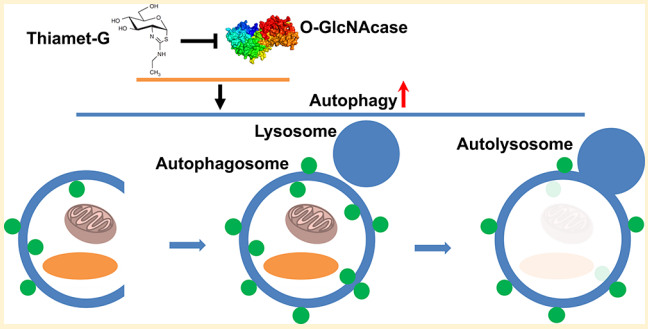

KEYWORDS: *Alzheimer's disease, glycosylation, autophagy, neurodegeneration, O-GlcNAc, Thiamet-G*

INTRODUCTION

The rising incidence of Alzheimer's disease (AD) within the aging population is causing increased social and economic burden. Because no disease modifying therapies are yet available, there is great interest in understanding both the basic biological mechanisms contributing to AD as well as advancing possible therapeutic approaches to slow or stop the progression of AD. The two well established pathological hallmarks of the disease are the neurofibrillary tangles (NFTs) and amyloid plaques that form within the brain. NFTs are composed of paired helical filaments (PHFs) of the cytoskeletal protein tau,[1] whereas amyloid plaques stem from aggregation of a proteolytic fragment of the amyloid precursor protein (APP).[2,3] There is growing consensus that amyloid initiates the AD cascade while pathological tau species, such as tau oligomers, drive neuronal death.[4,5] The central role of tau is supported by the close correlation between tau pathology and neuronal degeneration as well as clinical progression of the disease.[6,7] Consistent with this view, mutations in tau have been directly linked to neurodegenerative diseases.[8,9] Notably, tau is subject to many post-translational modifications (PTMs),[10,11] a number of which are involved in its pathological oligomerization and subsequent assembly into PHFs and NFTs.[10−12]

Both tau[13−16] and APP[17] are modified with an intracellular form of glycosylation known as O-linked *N*-acetylglucosamine (O-GlcNAc). O-GlcNAc is a dynamic protein modification found on nuclear, cytoplasmic, and mitochondrial proteins.[18,19] Though found on hundreds of proteins, levels of this modification are principally controlled by only two enzymes.[18] O-GlcNAc is installed on the hydroxyl groups of specific serine and threonine residues[19] by the enzyme O-GlcNAc transferase (OGT) using UDP-GlcNAc as a sugar donor,[20] and its removal is catalyzed by O-GlcNAcase (OGA).[21] It has been proposed that impaired brain glucose utilization within AD brain diminishes O-GlcNAcylation and enables the formation of toxic protein species.[15] OGA inhibitors slow the removal of O-GlcNAc from proteins while OGT continues to act, which leads to decreased rates of turnover of O-GlcNAc on proteins and a net increase in global protein O-GlcNAcylation. A series of studies using OGA inhibitors to elevate global levels of O-GlcNAc within various transgenic models of AD have shown that such compounds can lower Aβ levels and plaque burden,[22,23] levels of pathological tau,[24−27] protect against neurodegeneration, and improve behavior without causing apparent toxicity.[22−28] These promising findings have driven interest in using potent and selective OGA inhibitors as potential disease-modifying therapeutics for AD and other tauopathies, recently attracting attention from industry, which has advanced compounds to the clinic.[29]

The mechanisms by which OGA inhibitors decrease Aβ and tau pathologies and exert protective effects within the brain, however, remain ill defined. As noted, tau has been found to be O-GlcNAc modified[13−16] and O-GlcNAcylated tau is less prone to aggregation.[24] OGA inhibitors may therefore act directly by increasing tau glycosylation and hindering its downstream toxic effects. Others, however, have proposed that tau is not O-GlcNAc modified[26] or that the fraction of tau modified in this way is low.[10] Moreover OGA inhibitors have beneficial effects on behavior in tauopathy mouse models, even after short-term treatment, which seem unlikely to stem only from blocking tau toxicity and so suggest that mechanisms other than direct modification of tau are operative.[26] Accordingly, we were motivated to consider potential mechanisms by which OGA inhibitors might be able to protect against such proteotoxicity.

Macroautophagy, referred to here simply as autophagy, is the process by which cytoplasmic constituents, including protein aggregates and organelles, are sequestered in double-membrane structures called autophagosomes and delivered to lysosomes for degradation.[30] Both Aβ and tau are now recognized as being cleared in part by autophagy and impaired autophagy has emerged as a feature of AD as well as other neurodegenerative diseases.[31] We were motivated by several reports showing that remediating autophagic failure,[32] or stimulating autophagic clearance, correlates with reduced numbers of aggregates of Aβ and tau and reduces neurodegeneration in AD mouse models.[33−36] Given the concordance in the effects on tau and Aβ pathologies observed using known autophagy enchancers[33−36] and OGA inhibitors,[23,24] coupled with emerging data using genetic methods that suggest the O-GlcNAc pathway influences autophagy,[37−40] we speculated that OGA inhibitors might exert their protective effects in AD mouse models by enhancing autophagy within brain.

To interrogate the potential protective mechanisms of OGA inhibitors, we set out to test whether OGA inhibition stimulates autophagic flux within brain. Here, we show that OGA inhibitors act though an mTOR-independent manner to enhance autophagosome formation and increased autophagic flux both in vitro in immortal neuroblastoma cells and cultured primary neurons and astrocytes, as well as in vivo in mouse brain. We find that OGA inhibitors induced autophagy in two AD mouse models and that this correlates with reduced levels of pathological tau species. These results are consistent with the view that OGA inhibitors mediate their protective effects in AD, at least in part, by enhancing autophagy. Our findings here suggest OGA inhibitors should be generally protective in proteinopathy models in which induction of autophagy is beneficial. Moreover, the mTOR-independent nature of these effects is consistent with these compounds being well tolerated in AD mouse models and may open the door to more targeted strategies to induce autophagy within brain for therapeutic benefit.

RESULTS AND DISCUSSION

Given the great potential of OGA inhibitors as disease modifiers for treating tauopathies[22−28] and the advance of OGA inhibitors into the clinic,[29] an improved understanding of the processes by which OGA inhibitors affect cell physiology and associated cellular processes that could help combat tau toxicity are of great interest. Such knowledge should aid clinical development of OGA inhibitors and could also help uncover specific O-GlcNAcylated proteins that could be modulated in a more targeted manner for therapeutic benefit. Given that several papers have shown perturbations in O-GlcNAc levels have divergent effects on autophagy in various peripheral tissues[37−40] and that various autophagy enhancers decrease toxic tau species within tauopathy mouse models and provide protective benefits,[33−35,41,42] we set out to explore whether OGA inhibitors might stimulate autophagy in mammalian brain.

Inhibition of OGA Enhances Autophagy in Neuroblastoma Neuro-2a (N2a) Cells and Cultured Rat Primary Neurons and Astrocytes. Microtubule-associated protein 1 light chain 3 (LC3) is a ubiquitin-like modifier involved in autophagosome biogenesis. During the process of autophagy, pro-LC3 is processed to form LC3-I, which is subsequently conjugated to phosphatidylethanolamine (PE) to form LC3-II on the membrane of the phagophore where it promotes autophagosome formation. Following fusion of autophagosomes with lysosomes, intravacuolar LC3-II is degraded. Accordingly, monitoring the formation and degradation of LC3-II is a useful and well established measure for monitoring autophagy. Here, we selected the LC3B family member as an autophagy marker because of its abundance within brain[43] and monitored formation of LC3B−II (LC3BII). As a first step to explore whether inhibiting OGA influences autophagy in neurons, we used Neuro-2a (N2a) neuroblastoma cells as a convenient model system. We treated cells for 2 days with different concentrations of the OGA inhibitor Thiamet-G[44] (TMG) ranging from 25 nM to 250 μM and found increased levels of O-GlcNAc (Figure S1A). In the absence of bafilomycin A1, which blocks fusion of autophagosomes with lysosomes to form autolysosomes, we found no significant difference in the levels of LC3BII among cells treated with autophagy inducer rapamycin, different doses of TMG, and vehicle alone. In the presence of bafilomycin A1, the lowest does of TMG (25 nM) increased the level of LC3BII as compared with control, although the difference was not statistically significant (Figure S1B). Treatment with 100 nM TMG led to modest but statistically significant increases in

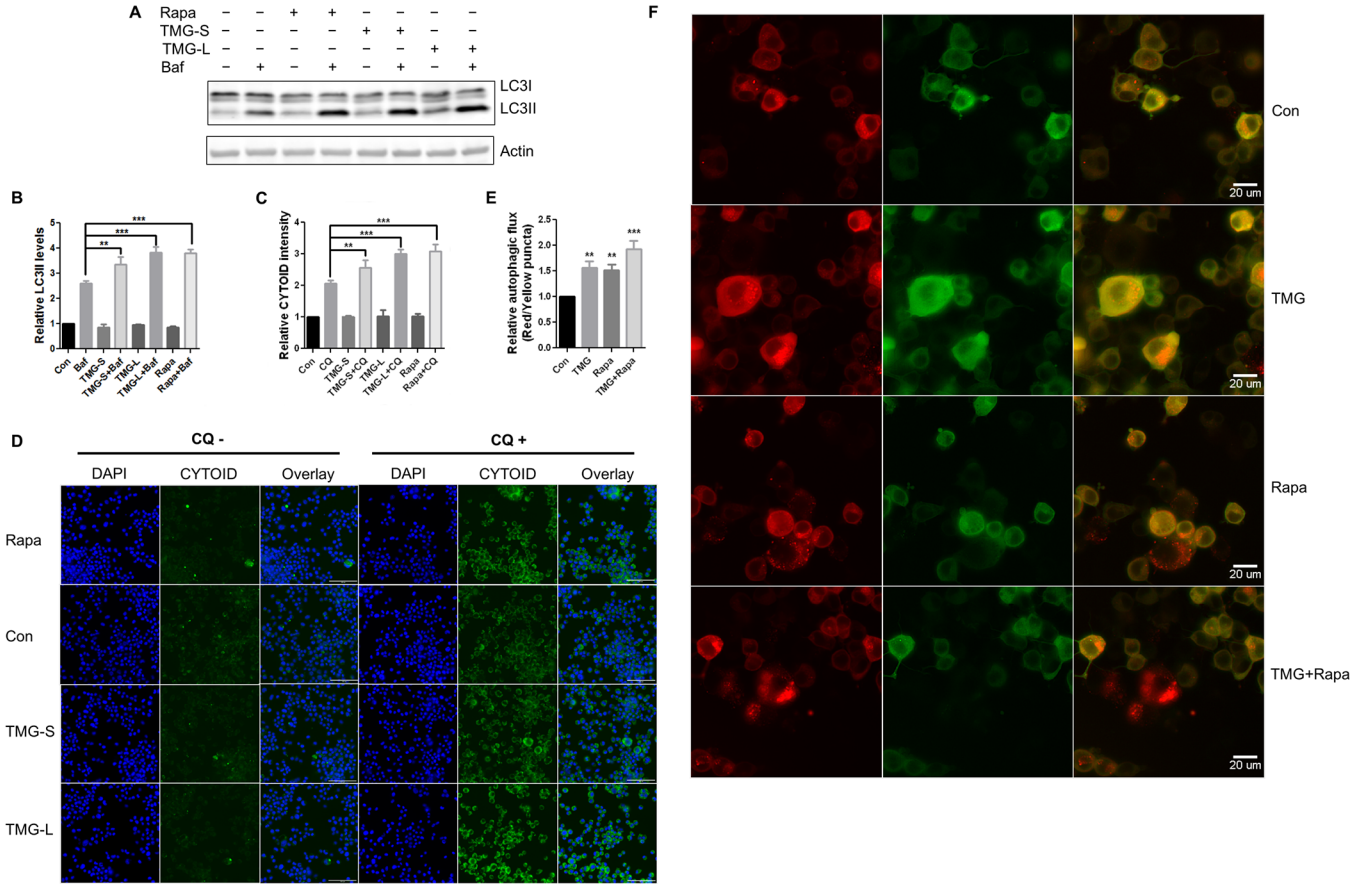

Figure 1. Inhibition of OGA by Thiamet-G (TMG) enhances autophagic flux in neuroblastoma Neuro-2a (N2a) cells. (A) Immunoblot analysis of levels of LC3BII in whole cell lysates from control and TMG-treated N2a cells. Con: vehicle control; Rapa: rapamycin, 2.5 μM for 4 h; TMG-S: TMG, 100 μM for 2 days; TMG-L: TMG, 100 μM for 15 days; Baf: bafilomycin A1, 100 nM for 4 h. (B) Densitometry of immunoblot signals in (A) was quantified using Odyssey software (Li-Cor). Values were normalized to corresponding beta-actin immunoblot signals, then normalized to control (arbitrarily set as 1). Error bars represent ± SD. *p*-Values were derived from a one-way analysis of variance (ANOVA) comparing immunoblot signals from each treatment to control, respectively. $n = 3$; $^{*}p < 0.05$, $^{**}p < 0.01$, $^{***}p < 0.001$. Treatments without significant differences were not labeled. (C) High-content cellular analysis of autophagic flux in live N2a cells using CYTO-ID Autophagy Detection Kit 2.0 (Enzo) which selectively labels autophagosomes. Con: vehicle control; Rapa: rapamycin, 2.5 μM for 4 h; TMG-S: TMG, 100 μM for 2 days; TMG-L: TMG, 100 μM for 15 days; CQ: Chloroquine, 25 μM for 4 h. Fluorescent signals from CYTOID staining of cells was quantified with automated methods using MetaXpress software (Molecular Devices). Error bars represent ± SD. *p*-Values were derived from a one-way analysis of variance (ANOVA) comparing fluorescent intensity of CYTOID staining from each treatment to control, respectively. $n = 3$; $^{*}p < 0.05$, $^{**}p < 0.01$, $^{***}p < 0.001$. (D) Representative images of high-content cellular analysis in (C). (E) Evaluation of autophagic flux in live N2a cells stably expressing tandem fluorescent protein pHluorin-mKate2-LC3 measured by high-content imaging (ImageXpress Micro XLS, Molecular Devices). Con: vehicle control; Rapa: rapamycin, 2.5 μM for 4 h; TMG: Thiamet-G, 100 μM for 15 days; TMG+Rapa: TMG, 100 μM for 15 days and Rapa, 2.5 μM for 4 h. Red and yellow puncta number per cell was automatically quantified using MetaXpress software. Error bars represent ± SD. *p*-Values were derived from a one-way analysis of variance (ANOVA) comparing the ratio of red/yellow puncta number per cell from each treatment to control, respectively. $n = 3$; $^{*}p < 0.05$, $^{**}p < 0.01$, $^{***}p < 0.001$. (F) Representative images of high-content imaging analysis in (E).

LC3BII level as compared with vehicle alone, and this effect on LC3BII levels was comparable to treatment with rapamycin (Figure S1B). These data suggest that OGA inhibition by TMG enhances autophagy within N2a cells. To address whether longer term OGA inhibition can induce sustained levels of autophagy, we next treated N2a cells with TMG for 15 days with 250 nM or 100 μM Thiamet-G followed by inhibition of autophagosome-lysosome fusion through the addition of bafilomycin A1 for 4 h. This long-term treatment significantly increased the levels of LC3BII as compared with vehicle alone (Figure 1A and B) and these effects on the levels of LC3BII were slightly greater than the shorter term 2-day dosing and were again comparable to the effect of rapamycin (Figure 1A and B). These data indicated that TMG could activate autophagy in a sustained manner. To confirm these findings, we used high-content cellular analysis to assess autophagic flux in live N2a cells treated with either 250 nM or 100 μM TMG using CYTO-ID (Enzo Life Sciences), which selectively stains autophagosomes and enables their quantitation by fluorescence imaging. CYTO-ID imaging revealed that rapamycin and TMG, with either a short (2 days) or long (15 days) treatment protocol, enhanced autophagy as compared to vehicle-treated cells, this time using the autophagy inhibitor chloroquine (CQ). These data are consistent with our immunoblot analyses of LC3BII and reveal activation of autophagy by TMG at both concentrations of 250 nM and 100 μM (Figure 1C and D). In this experiment we again observed that long-term (15 day) TMG treatment induced a higher level of autophagic flux than short-term (2 day) treatment (Figure 1C and D). As a further test, we exploited the established tandem reporter system based

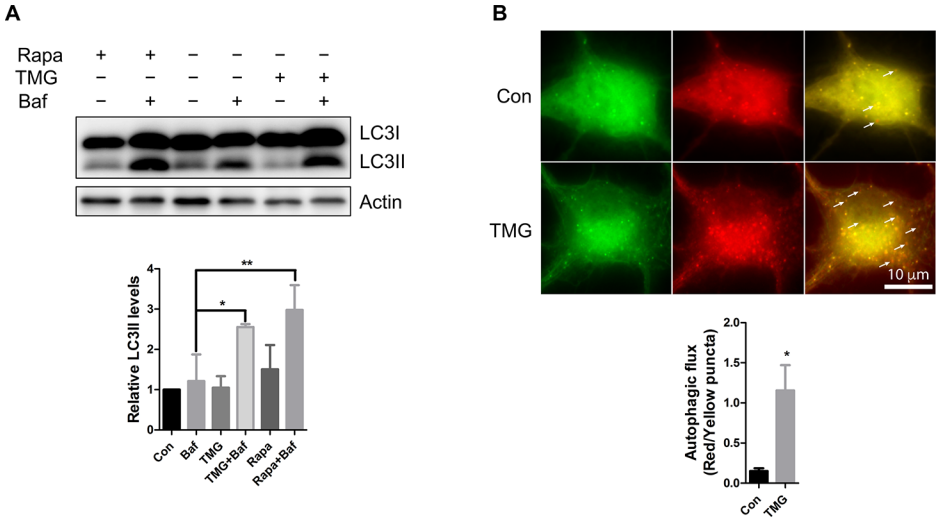

Figure 2. OGA inhibition by Thiamet-G (TMG) promotes autophagic flux in cultured rat primary neurons. (A) Immunoblot analysis of levels of LC3BII in whole cell lysates from control and TMG-treated primary cortical neurons. Con: vehicle control; Rapa: rapamycin, 0.2 μM for 72 h; TMG: Thiamet-G, 100 μM for 72 h; Baf: bafilomycin A1, 100 nM for 4 h. Densitometry of immunoblot signals was quantified using Odyssey software (Li-Cor). Values were normalized to corresponding beta-actin immunoblot signals, then normalized to control (arbitrarily set as 1). Error bars represent ± SD. p-Values were derived from a one-way analysis of variance (ANOVA) comparing immunoblot signals from each treatment to control, respectively. n = 3 independent cultures; $^{*}p < 0.05$, $^{**}p < 0.01$, $^{***}p < 0.001$. Treatments without significant differences were not labeled. (B) Evaluation of autophagic flux in live primary hippocampal neurons transiently expressing tandem fluorescent protein pHluorin-mKate2-LC3 using fluorescence microscopy. Con: vehicle control; TMG: Thiamet-G, 100 μM for 72 h. Red and yellow puncta number per cell were quantified using at least 20 cells per culture and per condition. Error bars represent ± SD. $^{*}p < 0.05$ by unpaired Student's t test (n = 3). Arrows denote mKate2 (red) positive structures.

on using the autophagy maker protein LC3 as a fusion with two fluorescent proteins having orthogonal photophysical properties (pHluorin-mKate2-LC3)[45] to generate an N2a cell line stably expressing this system. We treated this cell line with 250 nM or 100 μM of TMG for 15 days and assessed the extent of autophagic flux using high-content imaging analysis. Here too we found that both 250 nM and 100 μM TMG significantly increased autophagic flux presented as the ratio of red/yellow puncta per cell as compared with control (Figure 1E and F), with the increase being again comparable as seen when using rapamycin. Notably, we also observed greater autophagic flux in cells cotreated with both TMG and rapamycin as compared to cells treated with either TMG or rapamycin only (Figure 1E and F), suggesting these agents act through independent pathways to yield an additive enhancement in autophagic flux. To confirm that the enhancement of autophagy stems from OGA inhibition rather than some potential off-target effect of Thiamet-G, we tested two other structurally distinct OGA inhibitors[46] synthesized in-house at 250 nM. Both OGA inhibitors activated autophagy to a similar extent as TMG (Figure S2). These collective data support inhibition of OGA enhancing autophagy in N2a cells.

We next set out to evaluate the effect of OGA inhibition on autophagy in cultured rat primary neurons and astrocytes, which are more physiologically relevant models. Again, in the absence of bafilomycin, we observed no significant difference in the levels of LC3BII among control, rapamycin, and TMG treatments (3 day) as measured by immunoblot. However, after blocking autophagy using bafilomycin, LC3BII level increased significantly in the treatment with TMG (100 μM) as compared to cells treated with vehicle alone (Figure 2A). The effect of TMG on LC3BII was similar to that of the autophagy enhancer rapamycin (Figure 2A), supporting OGA inhibition induces autophagy in primary neurons. To confirm the enhancement of autophagic flux by TMG using a separate measure, we transiently transfected primary neurons with the tandem fluorescent reporter pHluorin-mKate2-LC3, and measured autophagic flux by fluorescence microscopy. We found that TMG treatment significantly increased autophagic flux shown as the ratio of red/yellow puncta number as compared with control (Figure 2B). Similar to primary neurons, we found that TMG treatment also raised the level of LC3BII in rat primary astrocytes after blocking formation of autolysosomes (Figure S3), suggesting induction of autophagy by TMG in astrocytes. These data together indicate that inhibition of OGA may promote autophagy within brain.

Inhibiting OGA Enhances Autophagic Flux in the Brain of RFP-GFP-LC3 Autophagy Reporter Mice. To address whether TMG influences autophagy within brain in vivo, we used as a model system the transgenic mouse strain CAG-RFP-EGFP-LC3 (C57BL/6-Tg(CAG-RFP/GFP/Map1lc3b)1Hill/J), which constitutively expresses the autophagy marker protein LC3 tagged with tandem fluorescent proteins (RFP-EGFP-LC3).[47] After the treatment of mice with TMG (500 mg/kg/d) in drinking water for 2 weeks, we found that the number of autophagosomes (yellow puncta) in the cortex was comparable between control and treated mice, whereas the number of autophagolysosome (red puncta) significantly increased in treated mice compared over the observed number in control mice (Figure 3A). TMG treatment also significantly increased autophagic flux as measured by the increased ratio of red/yellow puncta in treated mice as compared to controls (Figure 3A). Similar results were observed in other brain regions including brain stem and hippocampus (data not shown). These observations indicated that blocking OGA activity by TMG enhanced autophagic flux within mouse brain. To consolidate these imaging data, we also assessed the levels of Sequestosome-1 (SQSTM1), LC3BII and

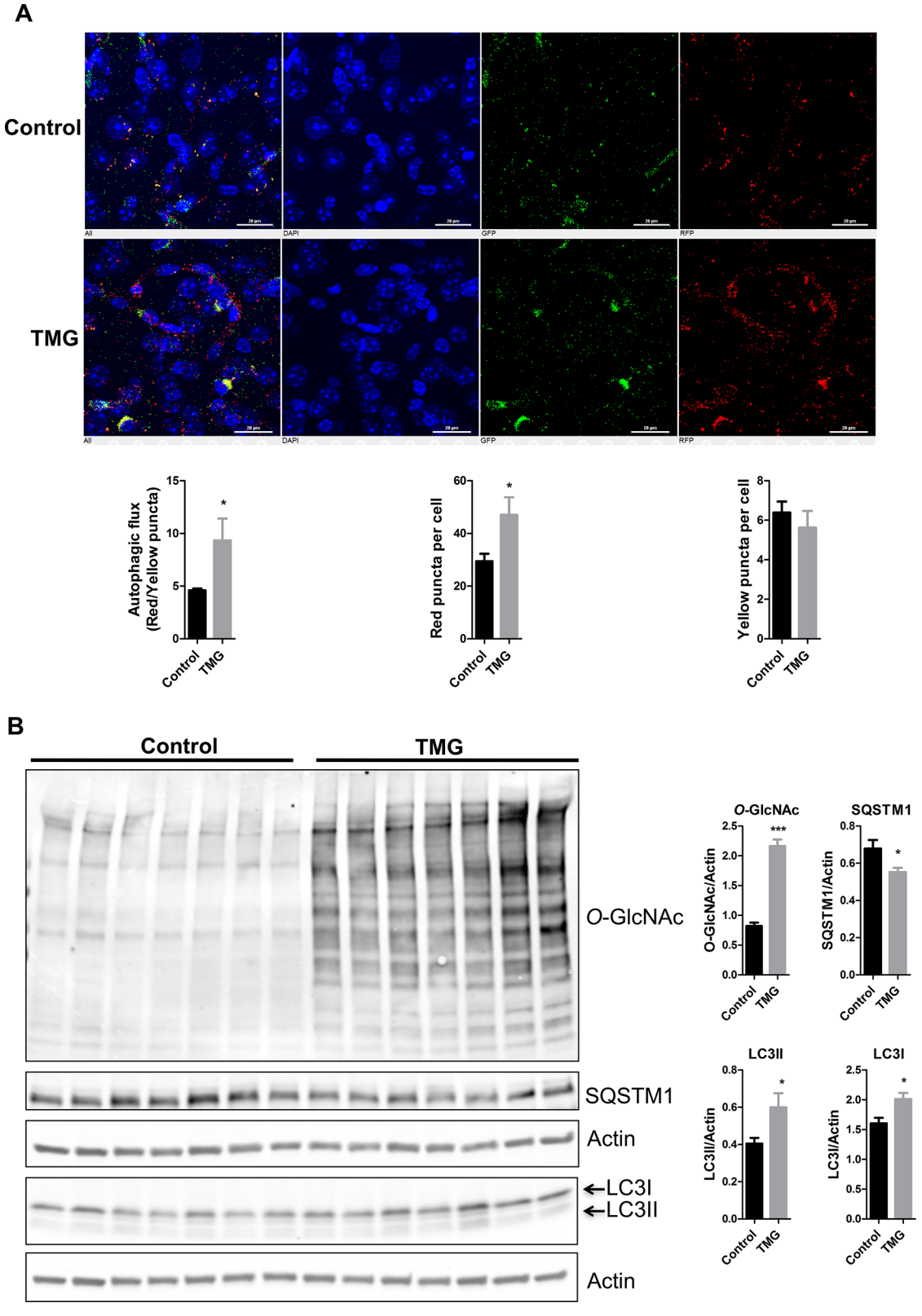

Figure 3. Increasing O-GlcNAc by using the selective OGA inhibitor Thiamet-G (TMG) enhances autophagic flux within brains of RFP-EGFP-LC3 mice. (A) Fluorescence analysis of the cortex region of sagittal sections from control and TMG-treated (500 mg/kg/d in drinking water for 2 weeks) mice constitutively expressing the tandem fluorescent autophagy maker protein RFP-EGFP-LC3. Numbers of red (autolysosome) and yellow (autophagosome) puncta were quantified using Nikon NIS-element software. Error bars represent ± SD. *$p < 0.05$ by unpaired Student's t test ($n = 7$). Comparisons that were not significantly different are unlabeled. (B) Immunoblot analysis of levels of O-GlcNAc, SQSTM1, and endogenous LC3I and LC3II in cortex lysate samples from control and TMG-treated RFP-EGFP-LC3 mice. Immunoblot signals were quantified using Odyssey software (Li-Cor). Values of immunoblot signals were normalized to those of corresponding beta-actin signals. Error bars represent ± SD. *$p < 0.05$, **$p < 0.01$, ***$p < 0.001$ by unpaired Student's t test ($n = 7$).

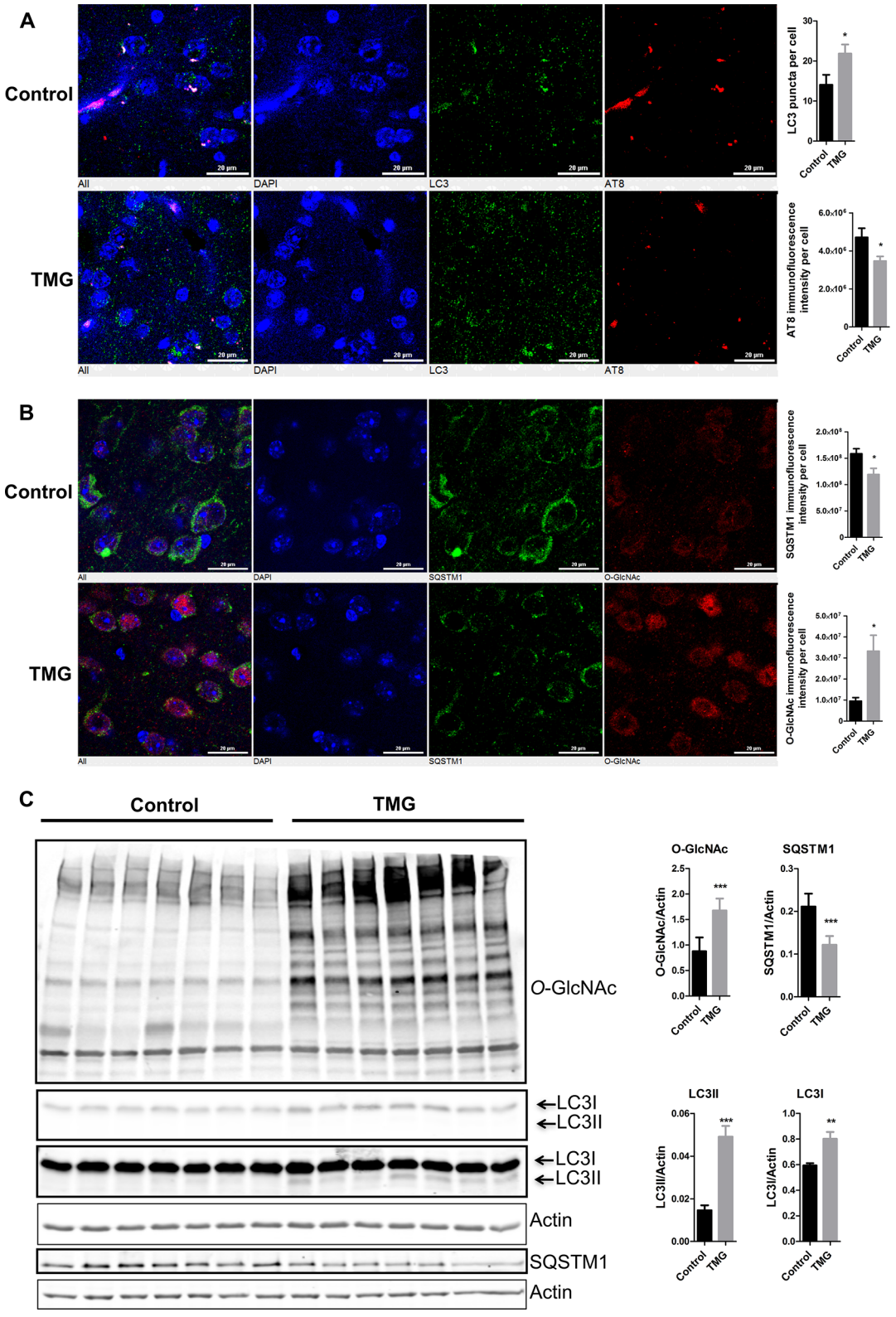

Figure 4. OGA inhibition by Thiamet-G (TMG) stimulates autophagy in AD mouse (JNPL3-Tau4R0NP301L) brain. Fluorescent immunohistochemical analysis of the cortex region using sagittal sections from control and TMG-treated (500 mg/kg/d in drinking water for 36 weeks) JNPL3 mice as measured using anti-LC3 and anti-pathological tau (AT8) antibodies (A), or anti-SQSTM1 and anti-O-GlcNAc (CTD110.6) antibodies (B). Immunofluorescence signals were quantified using Nikon NIS-element software. Error bars represent ± SD. *$p < 0.05$, **$p < 0.01$, ***$p < 0.001$ by unpaired Student's t test ($n = 7$). (C) Immunoblot analysis of levels of O-GlcNAc, LC3BI, LC3BII, and SQSTM1 in cortex lysate samples from control and TMG-treated JNPL3 mice. Immunoblot signals were quantified using Odyssey software (Li-Cor). Values of immunoblot signals were normalized to those of corresponding beta-actin signals. Error bars represent ± SD. *$p < 0.05$, **$p < 0.01$, ***$p < 0.001$ by unpaired Student's t test ($n = 7$).

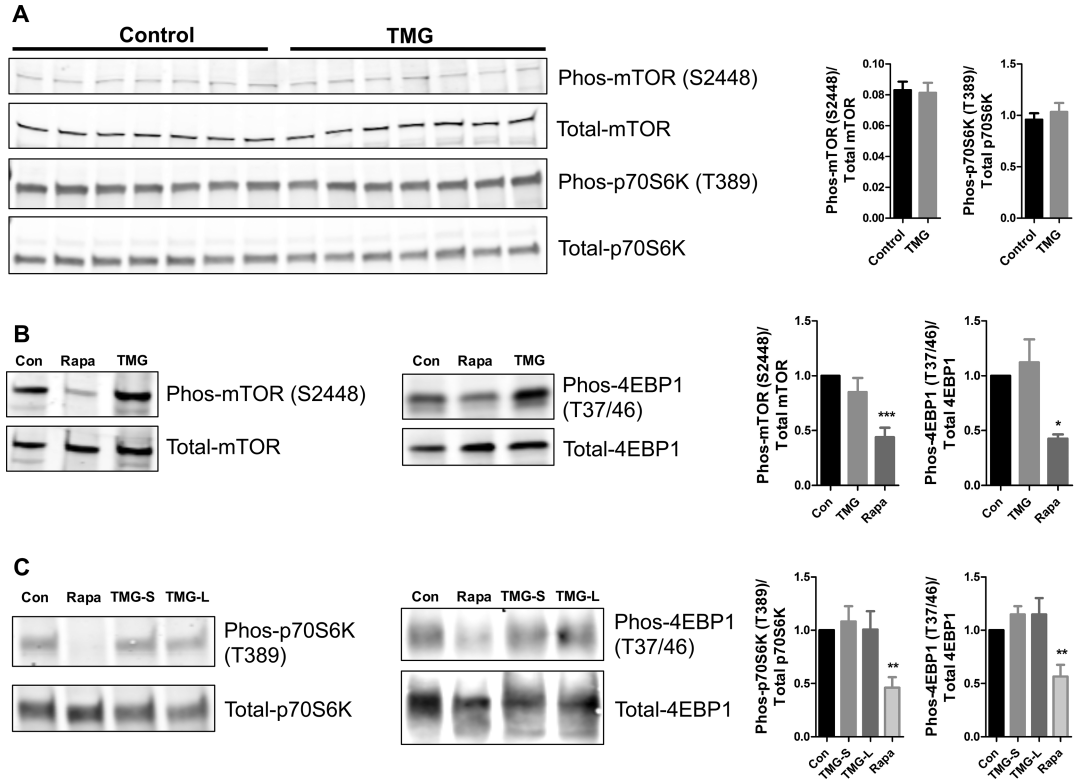

Figure 5. Thiamet-G (TMG) enhances autophagy through an mTOR-independent pathway. (A) TMG treatment did not alter the activity of mTOR in the brains of JNPL3 mice treated with TMG for 36 weeks. Immunoblot analysis of levels of total and phosphorylated epitopes of mTOR and p70S6K in cortex lysate samples from control and TMG-treated JNPL3 mice. Immunoblot signals were quantified using Odyssey software (Li-Cor). The ratio between the corresponding phosphorylated epitope and total protein was determined. Error bars represent ± SD. $*p < 0.05$, $**p < 0.01$, $***p < 0.001$ by unpaired Student's t test ($n = 7$). Comparison not showing significant differences are unlabeled. (B) Immunoblot analysis of levels of total and phosphorylated epitopes of mTOR and 4EBP1 in rat primary cortical neurons. Con: vehicle control; Rapa: rapamycin, 0.2 μM for 72 h; TMG: Thiamet-G, 100 μM for 72 h. The ratio between the corresponding phosphorylated epitope and total protein was determined, and then normalized to control (arbitrarily set as 1). Error bars represent ± SD. p-Values were derived from a one-way analysis of variance (ANOVA). $n = 3$; $*p < 0.05$, $**p < 0.01$, $***p < 0.001$. (C) Immunoblot analysis of levels of total and phosphorylated epitopes of p70S6K and 4EBP1 in N2a cells. Rapa: rapamycin, 2.5 μM for 4 h; TMG-S: TMG, 100 μM for 2 days; TMG-L: TMG, 100 μM for 15 days. The ratio between the corresponding phosphorylated epitope and total protein was determined, and then normalized to control (arbitrarily set as 1). Error bars represent ± SD. p-Values were derived from a one-way analysis of variance (ANOVA). $n = 3$; $*p < 0.05$, $**p < 0.01$, $***p < 0.001$.

O-GlcNAc using immunoblotting. SQSTM1 is an autophagy receptor, which can recognize and recruit specific cargoes for autophagic degradation. SQSTM1 is degraded during the process of autophagy and thus levels of SQSTM1 can serve, when used in conjunction with other measures, as another marker to aid in assessing autophagic flux. We found that OGA inhibition significantly increased the levels of O-GlcNAc and LC3BII, but decreased the level of SQSTM1 (Figure 3B). These immunoblot data are consistent with the imaging data described above and indicated that OGA inhibition by TMG promoted autophagy in the brain.

Pharmacological Inhibition of OGA Enhances Autophagy and Reduces Pathological Tau Species in Alzheimer's Disease Mouse Brain. Previous studies showed that OGA inhibition protects against neurodegeneration in the brain of various AD model mice.[22−27] Given that our *in vitro* and *in vivo* studies described above indicate inhibition of OGA activates autophagy, and that previous studies have shown that other methods that upregulate autophagic flux slow neurodegeneration,[33−35,41,42] we speculated that the protective function of TMG in tauopathy model mice might be mediated by enhanced autophagy. In order to test this hypothesis, we used JNPL3 tau transgenic mice that express mutant human tau P30lL[48] as a tauopathy model. Our previous study showed that long-term (36 weeks) TMG treatment hindered the formation of tau aggregates and decreases neuronal cell loss in JNPL3 mouse.[24] Here, using the same mouse model and treatment conditions[24] (500 mg/kg/day of TMG in drinking water over 36 weeks), we assessed autophagy in the brain using immunofluorescence. We observed that the number of LC3B immunoreactive puncta increased, whereas the intensity of SQSTM1 immunoreactivity in cortex was decreased in TMG-treated mice as compared to control mice (Figure 4A). These data are consistent with our observations made in RFP-EGFP-LC3 mouse brain and support OGA inhibition inducing persistent increases in autophagic flux within mouse brain. In addition, we found that levels of pathological tau as detected by AT-8 antibody decreased significantly, whereas O-GlcNAc immunoreactivity was greatly increased within the cortex of brains from TMG-treated mice (Figure 4A), which is in accord with previous studies by us and others.[24] We also observed both enhanced autophagy and a reduction in the levels of pathological tau, as measured using the AT-8 antibody, in other brain regions including both brain stem and hippocampus in TMG-treated mice (data not shown). These data together collectively indicate that OGA inhibition by TMG enhanced autophagic flux in mouse brain, and may contribute to clearing pathological tau species and thereby protecting against its

spread. In order to draw comparison with our studies described above, we measured the levels of O-GlcNAc, and the levels of standard autophagy markers including LC3BI, LC3BII, and SQSTM1 by immunoblot. All except SQSTM1 showed increased levels in TMG treated mice as compared to those treated with vehicle alone (Figure 4B). These immunoblot results are consistent with the immunofluorescence data in the JNPL3 mice as well as the RFP-EGFP-LC3 tandem reporter mice.

To evaluate the effects of shorter term dosing of TMG on autophagy in brain and confirm OGA inhibition influences autophagy in another AD model, we opted to use the 3×Tg-AD which harbors human tau (P301L), APP (KM670/671NL) and PS1 (M146V) mutant transgenes.[49] We treated these mice with either TMG (500 mg/kg/day) or vehicle alone in drinking water, as before but for only 2 weeks, and then assessed autophagy in the mouse brain using immunofluorescence. We found that both the number of LC3 puncta and SQSTM1 immunoreactivity were significantly reduced in cortex regions of TMG-treated mice as compared with control mice (Figure S4A). Notably, we also found that OGA inhibition with TMG reduced the levels of pathological tau as detected using the AT-8 antibody, whereas O-GlcNAc immunoreactivity was greatly increased in cortex (Figure S4A). Similar alterations in the number of LC3 puncta, levels of SQSTM1, and pathological tau were observed in other brain regions of TMG-treated mice including brain stem and hippocampus (data not shown). Unlike in JNPL3 mouse, however, we found that this shorter term OGA inhibition decreased the number of LC3 puncta in 3×Tg-AD as compared to control mice, yet the level of SQSTM1 was significantly reduced after TMG treatment to a similar extent as we had observed in the JNPL3 mice. This difference may be attributable to more robust autophagic flux including faster fusion between autophagosomes and lysosomes as well as higher lysosomal degradation capacity in the brains of these 3×Tg-AD mice, though this remains speculative. Nevertheless, these data support the view that OGA inhibition by TMG enhanced autophagy in the brain of these 3×Tg AD model mouse, which may be a factor driving the clearance of toxic tau species. Again, to use a separate method, we performed immunoblot analyses and found that levels of O-GlcNAc were significantly increased, whereas the levels of LC3BII, LC3BI and SQSTM1 were all decreased in the brain of mice treated with TMG as compared with control mice (Figure S4B) – findings that are in accord with the immunofluorescence data.

Thiamet-G (TMG) Enhances Autophagy through an mTOR-Independent Pathway. Noteworthy is that mTOR is present in two functionally distinct complexes, namely mTOR complex 1 (mTORC1) and mTORC2. mTORC1 is well-known as one of the key negative regulators of autophagy, while the role of mTORC2 in the direct regulation of autophagy is still ill-defined.[50] Therefore, our study here focused on the clearly understood pathway involving mTORC1 and do not rule out involvement of mTORC2. After determining that OGA inhibition with TMG activates autophagy both in vitro and in vivo, we set out to study whether TMG stimulates autophagy through an mTORC1-dependent or mTORC1-independent pathway. To this end, we analyzed by immunoblot the phosphorylation status of mTOR as well as mTORC1 substrate proteins p70S6K and 4EBP1. TMG treatment did not alter phosphorylation of mTOR at Ser^{2448} and p70S6K at Thr^{389} in brains of JNPL3 mice treated with TMG for 36 weeks (Figure 5A) nor in the brains of CAG-RFP-EGFP-LC3 mice treated with TMG for 2 weeks (Figure S5). Furthermore, TMG treatment induced no significant differences relative to controls in the extent of phosphorylation of either mTOR at Ser^{2448} or 4EBP1 at $Thr^{37/46}$ in rat primary cortical neurons (Figure 5B). Likewise, neither two day nor 15 day treatments with TMG impacted the extent of phosphorylation of p70S6K at Thr^{389} and 4EBP1 at $Thr^{37/46}$ in N2a cells (Figure 5B). Collectively, these cell and animal data indicated that inhibition of OGA does not influence the activity of mTORC1 and that TMG induces autophagy through an mTORC1-independent pathway in these contexts.

Because AMPK is one of the master regulators of autophagy, and the O-GlcNAc pathway has been proposed to interact with AMPK,[51] we wondered whether stimulation of autophagy by OGA inhibition might be mediated through AMPK. We therefore used immunoblot to analyze the phosphorylation status of both AMPK and AMPK substrate protein ULK1, the autophagy-initiating kinase. For neither protein, however, did we see a significant difference in phosphorylation as assessed in the brain of JNPL3 mouse, rat primary cortical neurons, and N2a cells when using site specific antibodies directed toward Thr^{172} of AMPK and Ser^{317} of ULK1 (Figure S6). These data suggest OGA inhibition does not alter the activity of either AMPK or ULK1 in neurons or neuronal models.

Tolerability and General Toxicity of Thiamet-G (TMG). During the preparation of this manuscript, Zhang and co-workers reported that inhibition of OGA by TMG reduces cell viability, activates mTOR, and blunts autophagic flux in primary rat cortical neurons.[52] They reported that treating rat primary cortical neurons with 25 μM TMG for 7 days greatly reduced cell viability as compared to control cells.[52] These surprising data are not in accord with our work described here, nor with previous reports from various laboratories that have used TMG. Indeed, previous studies carried out by independent groups have shown that systemic administration of TMG for up to 36 weeks does not result in any measurable neurotoxicity in different mouse models and, moreover, showed reproducible neuroprotective effects in AD mouse models.[22−28] Consistent with these reports, systemic administration of TMG in mice showed no obvious signs of toxicity either upon short-term (2 weeks) or long-term (36 weeks) treatments in this study. Further, we observed no toxicity associated with TMG in in various immortalized cell lines including N2a, SK-BR-3, MDA-MB-231, and HEK-293 treated with 25 or 100 μM TMG. In order to compare our experiments and studies with those of Zhang and co-workers[52] we performed cell viability assays using a more similar model. We found, however, no difference in the viability of rat primary cortical neurons treated for 7 days with vehicle alone or with TMG at concentrations of 25, 100, or 250 μM (Figure S7). Accordingly, our data, alongside that of others,[53] indicate that inhibition of OGA by TMG shows no neurotoxicity either in vitro or in vivo. We speculate that the differences between these collective observations and those of Zhang and co-workers may be attributable to the purity of TMG, which we prepared and characterized in house using a range of analytical methods (Figures S8 and S9). Alternatively, the effects may stem from the primary neurons used in our study being cocultured with an astrocyte feeder layer, which leads to more mature neurons with a higher synaptic density, as compared to Zhang and co-workers who cultured the primary neurons without an astrocyte feeder layer. Given these observations, we speculate that the effects of TMG on

autophagy in primary neurons as reported by Zhang and co-workers may stem from the conditions used, the purity of the TMG which was not described, or the methods used to assess autophagic flux. In this regard, it is notable that the Yang group reported recently that OGA inhibition by TMG stimulates autophagy in mouse primary hepatocytes[54] which though in different tissue is more consistent with our findings described here.

Regulation of Autophagy by the O-GlcNAc Pathway. It is interesting to compare and contrast our observations in brain with previous studies linking autophagy to perturbations in cellular O-GlcNAcylation. Our strategy used TMG as a selective inhibitor of OGA, which hinders the removal of O-GlcNAc from proteins. Because OGT continues to be active and add O-GlcNAc onto proteins, the rate of turnover of O-GlcNAc is decreased with the net result being a global increase in the levels of O-GlcNAcylated proteins within cells. Accordingly, TMG treatment is predicted to boost O-GlcNAcylation of many proteins including autophagy-related (ATG) proteins as well as other regulators of the autophagy pathway, which could accordingly alter autophagic flux. Though no previous studies have examined the effects of increasing O-GlcNAcylation in mammalian brain tissues, various groups have enhanced O-GlcNAcylation in other tissues using alternate strategies including treatment with high concentrations of a nonselective OGA inhibitor,[37] administration of glucosamine,[37] or overexpression of OGT.[39] In these studies conducted in murine cardiomyocytes and *Drosophila*, respectively, the treatments all led to reduced autophagy.[37,39] Decreasing O-GlcNAcylation by blocking formation of UDP-GlcNAc using broad spectrum aminotransferase inhibitors,[37] knock out of OGT,[38,40] overexpression of OGA,[55] or knockdown of OGT[38] all enhanced autophagy. More consistent with our study, reports have found that increasing O-GlcNAcylation by either knockout of OGA in *Caenorhabditis elegans*[40] or OGA inhibition using a nonselective OGA inhibitor in neuroblastoma SH-SY5Y cells[56] induces autophagy. Though these studies employ a range of tools and approaches in different model cells and organisms, they present a seemingly conflicting set of observations. We speculate this may be attributed to context dependency, the complexity of autophagy regulation, and the pleiotropic effects of O-GlcNAc being an abundant protein modification found on a diverse set of cellular proteins. Indeed, autophagy is a complex multistep processes, and can be regulated at different steps and through different pathways. There are more than 30 core ATG proteins that together initiate, promote, and complete autophagosome formation and degradation, as well as numerous proteins and pathways dedicated to regulating the process of autophagy.

A series of studies have implicated O-GlcNAcylation in regulation of autophagy through modification of specific proteins. Mutating identified O-GlcNAc sites in the autophagy regulator SNAP-29 was shown to promote autophagy, suggesting that increased O-GlcNAcylation of SNAP-29 may function to suppress autophagy.[38] In contrast, the O-GlcNAcylation of the cysteine protease ATG4B was proposed to increase its proteolytic activity and enhance autophagy[56] and O-GlcNAcylation of ULK1 and ULK2 was proposed to promote starvation-induced autophagy.[54] These specific studies, alongside those noted above, indicate that the overall outcome in terms of the downstream effects on autophagic flux may vary depending on the model and perturbation. Within specific tissues certain pathways may dominate regulation of autophagy, accounting for the apparently divergent sets of observations regarding regulation of autophagy by O-GlcNAc. These observations collectively suggest that regulation of autophagy by O-GlcNAc is a complex process that likely is tissue and environment specific.

CONCLUSION

In summary, genetic manipulation of O-GlcNAc levels have shown varied effects in a range of tissues but limited attention has been focused on brain, where OGA inhibitors have demonstrated utility in blocking neurodegeneration. Our data, in contrast to previous reports in vitro,[52] provides compelling evidence that OGA inhibition enhances autophagy in various neuronal models to a similar extent as the widely used autophagy enhancer rapamycin. Unlike rapamycin and its analogues, which can induce deleterious effects and therefore have limited potential in chronic indications due to their blockade of the mTOR pathway,[57−60] we find that OGA inhibitors activated autophagy through an mTOR-independent pathway as judged by evaluation of downstream markers of mTORC1 activity. The effects of OGA inhibition on mTORC2 activity are unknown, and cannot be ruled out by these studies. Importantly, and consistent with previous studies,[23,24,28] systemic administration of the OGA inhibitor Thiamet-G (TMG) at doses of up to 500 mg/kg/day resulted in no obvious signs of toxicity or behavioral deficits within our mouse studies noted during routine animal care or within cultured primary neurons. These findings collectively suggest that OGA inhibitors are potent and well tolerated compounds that can be used to perturb autophagy within the brain. Given the complexity of the pathways regulating and directly driving autophagy, alongside the large number of proteins known to be O-GlcNAc-modified within brain, it is likely that OGA inhibitors act to increase O-GlcNAc on diverse proteins that contribute to autophagic processes. Understanding these molecular mechanisms is an area of clear interest and such work should help uncover more targeted and efficient strategies to modify autophagy for therapeutic benefit through this important pathway. While headway has been made in this area as noted above,[38,54,56] a detailed understanding will require identifying the set of autophagy-related (ATG) proteins and autophagy regulators modified with O-GlcNAc, determining which of these are key players in specific tissue types, and ultimately establishing how O-GlcNAc influences the function of these key ATG proteins. Regardless of the precise mechanisms that are operative, our data provide clear support for TMG, and OGA inhibitors more generally, acting to enhance autophagy within brain.

Notably, enhancers of autophagy show benefit in a wide range of neurodegenerative diseases including Parkinson, Huntington, and Lou Gherig disease.[42] Moreover, OGA inhibitors have been found to offer protection against both amyloid toxicity in mouse models of disease[22,23] as well as in cellular models of Huntington disease.[61] Accordingly, we envision that TMG and other OGA inhibitors may serve to protect against a wide range of neurodegenerative diseases involving proteotoxicity. Given that OGA inhibitors have recently advanced into early clinical trials, our findings should stimulate interest in applying such compounds to other neurodegenerative diseases as well as driving the development of potential autophagy related biomarkers that could be used to support advancing OGA inhibitors in clinical studies. Finally, uncovering specific protein targets within brain that act via O-

GlcNAc to stimulate autophagy in an mTOR-independent manner may lead to more targeted strategies than global OGA inhibition.

METHODS

Reagents. Bafilomycin A1, rapamycin, and chloroquine were purchased from Sigma-Aldrich. Thiamet-G (TMG) was synthesized and characterized as described previously.[44]

Cell Culture and Treatment. Immortalized cell lines including N2a, SK-BR-3, MDA-MB-231, and HEK-293 were cultured in minimum essential medium (MEM) without L-glutamine (Thermo Fisher Scientific, 11090081) with 2 mM GlutaMAX (Thermo Fisher Scientific, 35050061), 10% (v/v) fetal bovine serum (FBS, Gibco), and 1% (v/v) penicillin/streptomycin at 37 °C in a water-jacketed, humidified CO_2 (5%) incubator. Cells were treated with TMG at indicated concentrations for 2 or 15 days. As a positive control, 2.5 μM rapamycin was added into assigned cell cultures 4 h before collection of lysates. To inhibit autophagy, cells were incubated with 100 nM bafilomycin A1 (Sigma) or 25 μM chloroquine for 4 h.

Embryonic day 18 (E18) rat primary hippocampal neurons and astrocytes were prepared exactly as described previously[62] and cultured in primary neuron growth media (PNGM; Lonza). The astrocyte feeder layer for the neuronal coculture was generated using neural progenitor cells as described.[63] For immunoblotting experiments, E18 cortical neurons were seeded in 6-well plates at a density of approximately 3.5×10^5 cells/well and prepared as described.[64] All experiments regarding the preparation of primary neurons and astrocytes were approved by and followed the guidelines set out by the Simon Fraser University Animal Care Committee: Protocol #943-B05. Ten days in vitro (DIV) cortical neurons were exposed to TMG treatment (100 μM) and rapamycin (0.2 μM). Neuronal cultures were then incubated for indicated experimental time points. Cell lysates were collected and subjected to immunoblot analysis.

Antibodies. The following primary antibodies were used in the Western blotting assays: anti-LC3B (Novus Biologicals, NB100-2220, 1:2000), anti-SQSTM1 (Sigam-Aldrich, P0067, 1:2000), anti-O-GlcNAc CTD110.6 (Biolegend, 838004, 1:3000), anti-beta-actin (Santa Cruz Biotechnology, sc-47778, 1:1000), anti-mTOR (Cell Signaling Technology, 2972S, 1:1000), anti-phospho-mTOR (Ser2448) (Cell Signaling Technology, 2971S, 1:1000), anti-p70S6K (Cell Signaling Technology, 2708S, 1:1000), anti-phospho-p70S6K (Thr389) (Cell Signaling Technology, 9205S, 1:1000), anti-4EBP1 (Cell Signaling Technology, 9452S, 1:1000), anti-phospho-4EBP1 (Thr37/46) (Cell Signaling Technology, 2855S, 1:1000), anti-AMPK Alpha (Cell Signaling Technology, 2532S, 1:1000), anti-phospho-AMPK alpha (Thr172) (Cell Signaling Technology, 2535S, 1:1000), anti-ULK1 (Cell Signaling Technology, 8054S, 1:1000), and anti-phospho-ULK1 (Ser317) (Cell Signaling Technology, 12753S, 1:1000).

Immunoblot Experiments. Protein samples were separated on 4 15% gradient SDS-PAGE gels (Bio-Rad) and transferred onto PVDF or nitrocellulose membrane (Bio-Rad). Membranes were blocked for 1 h in PBS-T (PBS, 0.1% Tween 20, pH 7.4) or PBS with 5% bovine serum albumin (BSA) (Bioshop) at room temperature, and then incubated with primary antibodies overnight at 4 °C. The following day, the membrane was rinsed thoroughly with PBS-T two times for 5 min and two times for 10 min. Membranes were then blocked with 3% BSA in PBS-T for 30 min at room temperature and then incubated with the IRDye 800CW or IRDye 680LT (Li-Cor) secondary antibody for 1 h at room temperature in dark followed by washing with PBS-T twice for 5 min and two times for 10 min. Finally, membranes were scanned using an Odyssey Infrared Imager (Li-Cor), and images were analyzed using Odyssey software (Li-Cor).

High-Content Imaging and Analysis. Cells were plated in 10 cm dishes at 10−25% confluency. One plate of cells was administered with 250 nM or 100 μM TMG immediately after plating. Spent media was replaced with fresh media containing 250 nM or 100 μM TMG every 2 days. Another plate of cells was cultured in the same way in parallel but with no inhibitor as a vehicle control. Thirteen days after plating, cells in these two 10 cm dishes were trypsinized and counted. Approximately 5000 cells were then seeded into each well of a 96-well plate (Corning 4680). Immediately after seeding, a subset of wells with cells from the vehicle control plate were treated with 250 nM or 100 μM TMG (TMG-S), whereas wells containing cells pretreated with TMG for 13 days continue to be treated with 250 nM or 100 μM TMG (TMG-L). Two days later, select wells of the 96-well plate were incubated with chloroquine and/or rapamycin (positive control) at indicated concentrations for 4 h. The whole plate of live cells was then stained with Hoechst 33342 (Thermo Fisher Scientific, H3570) and CYTO-ID dye (Enzo Life Sciences), which selectively labels autophagosomes according to the manufacturer's manual. Live cells in the plate were automatically imaged using high-content imaging (ImageXpress Micro XLS, Molecular Devices). Nine different nonoverlapping fields in each well were automatically selected and imaged. Images were automatically analyzed using software MetaXpress (Molecular Devices) to measure the number, area, and CYTO-ID staining intensity of autophagosomes. Cell lines stably expressing the fluorescent tandem reporter pHluorin-mKate2-LC3 (from Isei Tanida; Addgene plasmid # 61458) were cultured, treated and imaged live in a similar manner as described above. The number of both red (autolysosome) and yellow puncta (autophagosome) per cell was automatically quantified using software MetaXpress. Autophagic flux was presented as the ratio of red/yellow puncta.

Animals. All animal studies described below were approved by the Simon Fraser University Animal Care Committee. All animals were administrated TMG at a dose of 500 mg/kg/day. The TMG-treated group was dosed by including 3.75 mg/mL TMG in the drinking water bottles. This concentration was based on an average animal weight of 30 g and an average water consumption of 4 mL/day/animal. Both control and TMG-treated groups were allowed ad libitum access to food and water. Fourteen 9−12 week old hemizygous female JNPL3 mice (TgN(MAPT)JNPL3HlmcFemale) were obtained from Taconic. Animals were divided into two groups each containing seven animals, cohoused in groups of four or three in each cage, and allowed to acclimatize for 1 week prior to beginning the dosing regimen. JNPL3 mice were dosed with TMG for 36 weeks. Eight 36−40 week old female 3×Tg-AD "LaFerla mice" (tau (P301L), APP (KM670/671NL), and PS1 (M146V)) were a kind gift from Charles Krieger's lab at Simon Fraser University. These mice were divided into two groups each containing 4 animals, cohoused in groups of four in each cage, and allowed to acclimatize for 1 week prior to beginning the dosing regimen. LaFerla mice were dosed with TMG for 2 weeks. Fourteen 4−8 week old male RFP-GFP-LC3 mice (C57BL/6-Tg(CAG-RFP/GFP/Map1lc3b)1Hill/J) were purchased from the Jackson Laboratory. Animals were divided into two groups each containing seven animals, cohoused in groups of four or three in each cage, and allowed to acclimatize for 1 week prior to beginning the dosing regiment. RFP-GFP-LC3 mice were dosed with TMG for 2 weeks.

Animals were quickly sacrificed with CO_2 and perfused transcardially with 60 mL of saline solution. The brain was then quickly removed and the two hemispheres separated. The left hemisphere was placed into a solution of 4% paraformaldehyde (PFA). The right hemisphere was dissected on ice into the cortex, brainstem and hippocampus regions and quickly frozen in liquid nitrogen. At this point, all of the samples were relabeled with numbers in order to blind the investigators carrying out the analysis from the study groups. The codes were held separately until unblinding at the study end.

Brain tissues were homogenized in six volumes of tissue homogenization buffer (THB) containing 50 mM Tris-HCl pH 8, 1% (w/v) sodium dodecyl sulfate (SDS), 274 mM NaCl, 5 mM KCl, 2 mM EDTA, 2 mM EGTA, one complete-mini protease inhibitor tablet (Roche) per 50 mL, 5 mM sodium pyrophosphate, 30 mM β-glycerophosphate, 30 mM sodium fluoride, and 1 mM phenylmethylsulfonyl fluoride (PMSF) and then spun at 13,000*g* in an Eppendorf 5417C centrifuge for 20 min in the 4 °C cold-room. The resulting pellet was then re-extracted with three more volumes of THB and spun again at 13,000*g* for 20 min. The supernatants were then combined and referred to as brain lysates.

Fluorescence Microscopy. Following fixation of the brain in 4% PFA for 24 h the samples were transferred to 20% (w/v) sucrose overnight for cryoprotection. Brains were embedded in O.C.T. (Optimal Cutting Temperature) embedding medium (Sakura Finetek USA Inc.) and subsequently sectioned in the sagittal plane to generate 30 μm sections using a Leica cryostat. Free floating sections were permeabilized with 0.1 M PBS (pH 7.4) containing 0.3% Triton X-100 (PBST) for 15 min. After blocking with 10% normal goat serum (NGS) and 2.5% BSA in PBST for 60 min, sections were incubated with appropriate primary antibodies at 4 °C for 24 h. After washing with PBST for 45 min, sections were incubated with appropriate secondary antibodies conjugated with Alexa 488, Alexa 568, and Alexa 647 (Thermo Fisher Scientific) for 90 min. After 45 min washing, the sections were mounted on slides (Superfrost/Plus, Fisher), and coverslipped with Vectashield Mounting Medium with DAPI (H-1200, Vector Laboratories). Sections examined in parallel but without being exposed to primary antibody served as experimental controls. Stained brain sections were analyzed by a Nikon A1R laser scanning confocal system. For each brain section, images were acquired from three nonoverlapping fields at each neuroanatomic region including cortex, hippocampus, and brain stem using 40× or 60× oil-immersion objectives. Images were then analyzed using software NIS-Elements AR 3.1 (Nikon) to measure the number of LC3, GFP, and RPF puncta and quantify immunofluorescent intensity of SQSTM1, AT8, and O-GlcNAc.

For fluorescent imaging of autophagy in cultured primary hippocampal neurons, coverslips containing cortical neurons (10 DIV) were subjected to TMG treatment (100 μM) and transfected with tandem fluorescent reporter pHluorin-mKate2-LC3 using Endofectin according to the manufacturer's instructions (GeneCopoeia). Neurons were incubated for 24 h after transfection and then assessed by fluorescence microscopy (72 h exposure to TMG). As a negative control, bafilomycin A1 (100 nM, Sigma) was added to assigned coverslips 4 and 1 h before live imaging. Images were acquired using a Leica DMI6000B inverted epifluorescence microscope using a 63× 1.4 NA oil-immersion objective equipped with a cooled CCD camera controlled by MetaMorph (Molecular Devices). Tandem fluorescent reporter expressing neurons were mounted in a heated chamber (37 °C) and imaged live in both the GFP and RFP channels. Images of the GFP and RFP channels were merged in MetaMorph and the number of GFP+ and RFP+ puncta were scored in the cells treated with the indicated reagents.

Statistical Analysis. Statistical analyses were carried out using software Graphpad Prism 5.03. Data were analyzed using the unpaired Student's t test or one-way analysis of variance (ANOVA) when comparing more than two values. For all analysis, $p < 0.05$ was considered as statically significant. $^{*}p < 0.05$, $^{**}p < 0.01$, $^{***}p < 0.001$.

Pharmacological inhibition of OGA with different doses of TMG; other OGA inhibitors enhance autophagy in cells, OGA inhibitors enhance autophagy in primary rat astrocytes, TMG increases autophagy in 3xTg-AD mice, 2 week treamtent of mice does not alter mTOR activity in autophagy reporter mouse brain, OGA inhibition does not influence activity of AMPK or ULK1 in JNPL3 mouse brain, OGA inhibition with TMG does not affect viability of rat primary cortical neurons; ^{1}H NMR and ^{13}C NMR spectra; HPLC chromatogram of TMG; characterization of TMG (PDF)

AUTHOR INFORMATION

Corresponding Author

*E-mail: dvocadlo@sfu.ca.

ORCID

David J. Vocadlo: 0000-0001-6897-5558

Author Contributions

D.J.V., S.G., M.A.S. and Y.Z. designed experiments. Y.Z., X.S., F.S, N.E.G., N.L., A.S., M.C.H., M.D., V.H., R.A., and Z.M. conducted experiments. Y.Z., F.S., M.C.H., and M.A.S. analyzed data. Y.Z. and D.J.V wrote the manuscript, and all authors provided input into the manuscript.

Funding

This research was supported by funding from the Canadian Institutes of Health Research (CIHR Grant MOP-123341), Brain Canada, Genome British Columbia, the Michael Smith Foundation for Health Research, Pacific Alzheimer Research Foundation, the Natural Sciences and Engineering Research Council of Canada (NSERC, Grant 327100-2011), and the Canadian Glycomics Network (GlycoNet), a member of the Networks of Centres of Excellence Canada program. M.D. is supported by the Natural Sciences and Engineering Research Council of Canada as a doctoral fellow. D.J.V. is supported as a Tier I Canada Research Chair in Chemical Biology.

Notes

The authors declare the following competing financial interest(s): D.J.V. is a cofounder, CSO, Chair of the SAB, and holds equity in Alectos Therapeutics. X.S. and D.J.V. may receive royalties from SFU for commercialization of technology relating to OGA inhibitors.

ACKNOWLEDGMENTS

We thank A. Akram for assistance with neuronal culture preparations and technical assistance, T. Huynh for initial experiments, and the SFU Animal Care staff for assistance in the animal studies.

ABBREVIATIONS

4EBP1, eukaryotic translation initiation factor 4E-binding protein 1; AD, Alzheimer's disease; AMPK, 5′ adenosine monophosphate-activated protein kinase; ANOVA, analysis of variance; APP, amyloid precursor protein; ATG, autophagy related; LC3B, microtubule-associated protein 1 light chain 3 beta; NFT, neurofibrillary tangle; mTOR, mechanistic target of rapamycin; O-GlcNAc, O-linked *N*-acetylglucosamine; OGA, O-GlcNAcase; OGT, O-GlcNAc transferase; p70S6K, 70 kDa ribosomal protein S6 kinase 1; PHF, paired helical filament; PS1, presenilin-1; PTM, post-translational modification; SQSTM1, sequestosome-1; Tg, transgenic; TMG, Thiamet-G; ULK1, unc-51 like kinase 1; ULK2, unc-51 like kinase 2

REFERENCES

(1) Grundke-Iqbal, I., Iqbal, K., Tung, Y. C., Quinlan, M., Wisniewski, H. M., and Binder, L. I. (1986) Abnormal phosphorylation of the microtubule-associated protein tau (tau) in Alzheimer cytoskeletal pathology. *Proc. Natl. Acad. Sci. U. S. A. 83*, 4913−4917.

(2) Masters, C. L., Multhaup, G., Simms, G., Pottgiesser, J., Martins, R. N., and Beyreuther, K. (1985) Neuronal origin of a cerebral amyloid: neurofibrillary tangles of Alzheimer's disease contain the same protein as the amyloid of plaque cores and blood vessels. *EMBO J. 4*, 2757−2763.

(3) Kang, J., Lemaire, H. G., Unterbeck, A., Salbaum, J. M., Masters, C. L., Grzeschik, K. H., Multhaup, G., Beyreuther, K., and Muller-Hill,

B. (1987) The precursor of Alzheimer's disease amyloid A4 protein resembles a cell-surface receptor. *Nature 325*, 733−736.
(4) Musiek, E. S., and Holtzman, D. M. (2015) Three dimensions of the amyloid hypothesis: time, space and 'wingmen'. *Nat. Neurosci. 18*, 800−806.
(5) Bloom, G. S. (2014) Amyloid-beta and tau: the trigger and bullet in Alzheimer disease pathogenesis. *JAMA Neurol. 71*, 505−508.
(6) Mattsson, N., Scholl, M., Strandberg, O., Smith, R., Palmqvist, S., Insel, P. S., Hagerstrom, D., Ohlsson, T., Zetterberg, H., Jogi, J., Blennow, K., and Hansson, O. (2017) 18F-AV-1451 and CSF T-tau and P-tau as biomarkers in Alzheimer's disease. *EMBO Mol. Med. 9*, 1212−1223.
(7) Nelson, P. T., Alafuzoff, I., Bigio, E. H., Bouras, C., Braak, H., Cairns, N. J., Castellani, R. J., Crain, B. J., Davies, P., Del Tredici, K., Duyckaerts, C., Frosch, M. P., Haroutunian, V., Hof, P. R., Hulette, C. M., Hyman, B. T., Iwatsubo, T., Jellinger, K. A., Jicha, G. A., Kovari, E., Kukull, W. A., Leverenz, J. B., Love, S., Mackenzie, I. R., Mann, D. M., Masliah, E., McKee, A. C., Montine, T. J., Morris, J. C., Schneider, J. A., Sonnen, J. A., Thal, D. R., Trojanowski, J. Q., Troncoso, J. C., Wisniewski, T., Woltjer, R. L., and Beach, T. G. (2012) Correlation of Alzheimer disease neuropathologic changes with cognitive status: a review of the literature. *J. Neuropathol. Exp. Neurol. 71*, 362−381.
(8) Hutton, M., Lendon, C. L., Rizzu, P., Baker, M., Froelich, S., Houlden, H., Pickering-Brown, S., Chakraverty, S., Isaacs, A., Grover, A., Hackett, J., Adamson, J., Lincoln, S., Dickson, D., Davies, P., Petersen, R. C., Stevens, M., de Graaff, E., Wauters, E., van Baren, J., Hillebrand, M., Joosse, M., Kwon, J. M., Nowotny, P., Che, L. K., Norton, J., Morris, J. C., Reed, L. A., Trojanowski, J., Basun, H., Lannfelt, L., Neystat, M., Fahn, S., Dark, F., Tannenberg, T., Dodd, P. R., Hayward, N., Kwok, J. B., Schofield, P. R., Andreadis, A., Snowden, J., Craufurd, D., Neary, D., Owen, F., Oostra, B. A., Hardy, J., Goate, A., van Swieten, J., Mann, D., Lynch, T., and Heutink, P. (1998) Association of missense and 5′-splice-site mutations in tau with the inherited dementia FTDP-17. *Nature 393*, 702−705.
(9) Spillantini, M. G., Murrell, J. R., Goedert, M., Farlow, M. R., Klug, A., and Ghetti, B. (1998) Mutation in the tau gene in familial multiple system tauopathy with presenile dementia. *Proc. Natl. Acad. Sci. U. S. A. 95*, 7737−7741.
(10) Morris, M., Knudsen, G. M., Maeda, S., Trinidad, J. C., Ioanoviciu, A., Burlingame, A. L., and Mucke, L. (2015) Tau post-translational modifications in wild-type and human amyloid precursor protein transgenic mice. *Nat. Neurosci. 18*, 1183−1189.
(11) Song, L., Lu, S. X., Ouyang, X., Melchor, J., Lee, J., Terracina, G., Wang, X., Hyde, L., Hess, J. F., Parker, E. M., and Zhang, L. (2015) Analysis of tau post-translational modifications in rTg4510 mice, a model of tau pathology. *Mol. Neurodegener. 10*, 14.
(12) Marcus, J. N., and Schachter, J. (2011) Targeting post-translational modifications on tau as a therapeutic strategy for Alzheimer's disease. *J. Neurogenet. 25*, 127−133.
(13) Arnold, C. S., Johnson, G. V., Cole, R. N., Dong, D. L., Lee, M., and Hart, G. W. (1996) The microtubule-associated protein tau is extensively modified with O-linked N-acetylglucosamine. *J. Biol. Chem. 271*, 28741−28744.
(14) Lefebvre, T., Ferreira, S., Dupont-Wallois, L., Bussiere, T., Dupire, M. J., Delacourte, A., Michalski, J. C., and Caillet-Boudin, M. L. (2003) Evidence of a balance between phosphorylation and O-GlcNAc glycosylation of Tau proteins–a role in nuclear localization. *Biochim. Biophys. Acta, Gen. Subj. 1619*, 167−176.
(15) Liu, F., Iqbal, K., Grundke-Iqbal, I., Hart, G. W., and Gong, C. X. (2004) O-GlcNAcylation regulates phosphorylation of tau: a mechanism involved in Alzheimer's disease. *Proc. Natl. Acad. Sci. U. S. A. 101*, 10804−10809.
(16) Robertson, L. A., Moya, K. L., and Breen, K. C. (2004) The potential role of tau protein O-glycosylation in Alzheimer's disease. *J. Alzheimer's Dis. 6*, 489−495.
(17) Griffith, L. S., Mathes, M., and Schmitz, B. (1995) Beta-amyloid precursor protein is modified with O-linked N-acetylglucosamine. *J. Neurosci. Res. 41*, 270−278.
(18) Zachara, N., Akimoto, Y., and Hart, G. W. (2015) The O-GlcNAc Modification. In *Essentials of Glycobiology* (Varki, A., Cummings, R. D., Esko, J. D., Stanley, P., Hart, G. W., Aebi, M., Darvill, A. G., Kinoshita, T., Packer, N. H., Prestegard, J. H., Schnaar, R. L., and Seeberger, P. H., Eds.), 3rd ed., Cold Spring Harbor Laboratory Press, Cold Spring Harbor, NY.
(19) Torres, C. R., and Hart, G. W. (1984) Topography and polypeptide distribution of terminal N-acetylglucosamine residues on the surfaces of intact lymphocytes. Evidence for O-linked GlcNAc. *J. Biol. Chem. 259*, 3308−3317.
(20) Lubas, W. A., Frank, D. W., Krause, M., and Hanover, J. A. (1997) O-Linked GlcNAc transferase is a conserved nucleocytoplasmic protein containing tetratricopeptide repeats. *J. Biol. Chem. 272*, 9316−9324.
(21) Gao, Y., Wells, L., Comer, F. I., Parker, G. J., and Hart, G. W. (2001) Dynamic O-glycosylation of nuclear and cytosolic proteins: cloning and characterization of a neutral, cytosolic beta-N-acetylglucosaminidase from human brain. *J. Biol. Chem. 276*, 9838−9845.
(22) Yuzwa, S. A., Shan, X., Jones, B. A., Zhao, G., Woodward, M. L., Li, X., Zhu, Y., McEachern, E. J., Silverman, M. A., Watson, N. V., Gong, C. X., and Vocadlo, D. J. (2014) Pharmacological inhibition of O-GlcNAcase (OGA) prevents cognitive decline and amyloid plaque formation in bigenic tau/APP mutant mice. *Mol. Neurodegener. 9*, 42.
(23) Kim, C., Nam, D. W., Park, S. Y., Song, H., Hong, H. S., Boo, J. H., Jung, E. S., Kim, Y., Baek, J. Y., Kim, K. S., Cho, J. W., and Mook-Jung, I. (2013) O-linked beta-N-acetylglucosaminidase inhibitor attenuates beta-amyloid plaque and rescues memory impairment. *Neurobiol. Aging 34*, 275−285.
(24) Yuzwa, S. A., Shan, X., Macauley, M. S., Clark, T., Skorobogatko, Y., Vosseller, K., and Vocadlo, D. J. (2012) Increasing O-GlcNAc slows neurodegeneration and stabilizes tau against aggregation. *Nat. Chem. Biol. 8*, 393−399.
(25) Graham, D. L., Gray, A. J., Joyce, J. A., Yu, D., O'Moore, J., Carlson, G. A., Shearman, M. S., Dellovade, T. L., and Hering, H. (2014) Increased O-GlcNAcylation reduces pathological tau without affecting its normal phosphorylation in a mouse model of tauopathy. *Neuropharmacology 79*, 307−313.
(26) Borghgraef, P., Menuet, C., Theunis, C., Louis, J. V., Devijver, H., Maurin, H., Smet-Nocca, C., Lippens, G., Hilaire, G., Gijsen, H., Moechars, D., and Van Leuven, F. (2013) Increasing brain protein O-GlcNAc-ylation mitigates breathing defects and mortality of Tau.P301L mice. *PLoS One 8*, e84442.
(27) Hastings, N. B., Wang, X., Song, L., Butts, B. D., Grotz, D., Hargreaves, R., Fred Hess, J., Hong, K. K., Huang, C. R., Hyde, L., Laverty, M., Lee, J., Levitan, D., Lu, S. X., Maguire, M., Mahadomrongkul, V., McEachern, E. J., Ouyang, X., Rosahl, T. W., Selnick, H., Stanton, M., Terracina, G., Vocadlo, D. J., Wang, G., Duffy, J. L., Parker, E. M., and Zhang, L. (2017) Inhibition of O-GlcNAcase leads to elevation of O-GlcNAc tau and reduction of tauopathy and cerebrospinal fluid tau in rTg4510 mice. *Mol. Neurodegener. 12*, 39.
(28) Macauley, M. S., Shan, X., Yuzwa, S. A., Gloster, T. M., and Vocadlo, D. J. (2010) Elevation of Global O-GlcNAc in rodents using a selective O-GlcNAcase inhibitor does not cause insulin resistance or perturb glucohomeostasis. *Chem. Biol. 17*, 949−958.
(29) Smith, S. M., Struyk, A., Jonathan, D., Declercq, R., Marcus, J., Toolan, D., Wang, X., Schachter, J. B., Pearson, M., Hess, F., Selnick, H., Salinas, C., Li, W., Duffy, J., McEachern, E., Vocadlo, D. J., Renger, J. J., Eric, H. D., Forman, M., and Schoepp, D. (2016) Early clinical results and preclinical validation of the O-GlcNAcase (OGA) inhibitor MK-8719 as a novel therapeutic for the treatment of tauopathies. *Alzheimer's Dementia 12*, P261.
(30) Yang, Z., and Klionsky, D. J. (2010) Eaten alive: a history of macroautophagy. *Nat. Cell Biol. 12*, 814−822.
(31) Wong, E., and Cuervo, A. M. (2010) Autophagy gone awry in neurodegenerative diseases. *Nat. Neurosci. 13*, 805−811.
(32) Yang, D. S., Stavrides, P., Mohan, P. S., Kaushik, S., Kumar, A., Ohno, M., Schmidt, S. D., Wesson, D., Bandyopadhyay, U., Jiang, Y., Pawlik, M., Peterhoff, C. M., Yang, A. J., Wilson, D. A., George-Hyslop,

P., St, Westaway, D., Mathews, P. M., Levy, E., Cuervo, A. M., and Nixon, R. A. (2011) Reversal of autophagy dysfunction in the TgCRND8 mouse model of Alzheimer's disease ameliorates amyloid pathologies and memory deficits. *Brain 134*, 258−277.

(33) Ozcelik, S., Fraser, G., Castets, P., Schaeffer, V., Skachokova, Z., Breu, K., Clavaguera, F., Sinnreich, M., Kappos, L., Goedert, M., Tolnay, M., and Winkler, D. T. (2013) Rapamycin attenuates the progression of tau pathology in P301S tau transgenic mice. *PLoS One 8*, e62459.

(34) Schaeffer, V., Lavenir, I., Ozcelik, S., Tolnay, M., Winkler, D. T., and Goedert, M. (2012) Stimulation of autophagy reduces neurodegeneration in a mouse model of human tauopathy. *Brain 135*, 2169−2177.

(35) Li, L., Zhang, S., Zhang, X., Li, T., Tang, Y., Liu, H., Yang, W., and Le, W. (2013) Autophagy enhancer carbamazepine alleviates memory deficits and cerebral amyloid-beta pathology in a mouse model of Alzheimer's disease. *Curr. Alzheimer Res. 10*, 433−441.

(36) Spilman, P., Podlutskaya, N., Hart, M. J., Debnath, J., Gorostiza, O., Bredesen, D., Richardson, A., Strong, R., and Galvan, V. (2010) Inhibition of mTOR by rapamycin abolishes cognitive deficits and reduces amyloid-beta levels in a mouse model of Alzheimer's disease. *PLoS One 5*, e9979.

(37) Marsh, S. A., Powell, P. C., Dell'italia, L. J., and Chatham, J. C. (2013) Cardiac O-GlcNAcylation blunts autophagic signaling in the diabetic heart. *Life Sci. 92*, 648−656.

(38) Guo, B., Liang, Q., Li, L., Hu, Z., Wu, F., Zhang, P., Ma, Y., Zhao, B., Kovacs, A. L., Zhang, Z., Feng, D., Chen, S., and Zhang, H. (2014) O-GlcNAc-modification of SNAP-29 regulates autophagosome maturation. *Nat. Cell Biol. 16*, 1215−1226.

(39) Park, S., Lee, Y., Pak, J. W., Kim, H., Choi, H., Kim, J. W., Roth, J., and Cho, J. W. (2015) O-GlcNAc modification is essential for the regulation of autophagy in Drosophila melanogaster. *Cell. Mol. Life Sci. 72*, 3173−3183.

(40) Wang, P., and Hanover, J. A. (2013) Nutrient-driven O-GlcNAc cycling influences autophagic flux and neurodegenerative proteotoxicity. *Autophagy 9*, 604−606.

(41) Congdon, E. E., Wu, J. W., Myeku, N., Figueroa, Y. H., Herman, M., Marinec, P. S., Gestwicki, J. E., Dickey, C. A., Yu, W. H., and Duff, K. E. (2012) Methylthioninium chloride (methylene blue) induces autophagy and attenuates tauopathy in vitro and in vivo. *Autophagy 8*, 609−622.

(42) Menzies, F. M., Fleming, A., Caricasole, A., Bento, C. F., Andrews, S. P., Ashkenazi, A., Fullgrabe, J., Jackson, A., Jimenez Sanchez, M., Karabiyik, C., Licitra, F., Lopez Ramirez, A., Pavel, M., Puri, C., Renna, M., Ricketts, T., Schlotawa, L., Vicinanza, M., Won, H., Zhu, Y., Skidmore, J., and Rubinsztein, D. C. (2017) Autophagy and Neurodegeneration: Pathogenic Mechanisms and Therapeutic Opportunities. *Neuron 93*, 1015−1034.

(43) He, H., Dang, Y., Dai, F., Guo, Z., Wu, J., She, X., Pei, Y., Chen, Y., Ling, W., Wu, C., Zhao, S., Liu, J. O., and Yu, L. (2003) Post-translational modifications of three members of the human MAP1LC3 family and detection of a novel type of modification for MAP1LC3B. *J. Biol. Chem. 278*, 29278−29287.

(44) Yuzwa, S. A., Macauley, M. S., Heinonen, J. E., Shan, X., Dennis, R. J., He, Y., Whitworth, G. E., Stubbs, K. A., McEachern, E. J., Davies, G. J., and Vocadlo, D. J. (2008) A potent mechanism-inspired O-GlcNAcase inhibitor that blocks phosphorylation of tau in vivo. *Nat. Chem. Biol. 4*, 483−490.

(45) Tanida, I., Ueno, T., and Uchiyama, Y. (2014) A super-ecliptic, pHluorin-mKate2, tandem fluorescent protein-tagged human LC3 for the monitoring of mammalian autophagy. *PLoS One 9*, e110600.

(46) Quanttropani, A., Kulkarni, S. S., and Gajendra, A. (2016) Glycosidase Inhibitors. Patent WO2017144633A1.

(47) Li, L., Wang, Z. V., Hill, J. A., and Lin, F. (2014) New autophagy reporter mice reveal dynamics of proximal tubular autophagy. *J. Am. Soc. Nephrol. 25*, 305−315.

(48) Lewis, J., McGowan, E., Rockwood, J., Melrose, H., Nacharaju, P., Van Slegtenhorst, M., Gwinn-Hardy, K., Paul Murphy, M., Baker, M., Yu, X., Duff, K., Hardy, J., Corral, A., Lin, W. L., Yen, S. H., Dickson, D. W., Davies, P., and Hutton, M. (2000) Neurofibrillary tangles, amyotrophy and progressive motor disturbance in mice expressing mutant (P301L) tau protein. *Nat. Genet. 25*, 402−405.

(49) Oddo, S., Caccamo, A., Shepherd, J. D., Murphy, M. P., Golde, T. E., Kayed, R., Metherate, R., Mattson, M. P., Akbari, Y., and LaFerla, F. M. (2003) Triple-transgenic model of Alzheimer's disease with plaques and tangles: intracellular Abeta and synaptic dysfunction. *Neuron 39*, 409−421.

(50) Kim, Y. C., and Guan, K. L. (2015) mTOR: a pharmacologic target for autophagy regulation. *J. Clin. Invest. 125*, 25−32.

(51) Bullen, J. W., Balsbaugh, J. L., Chanda, D., Shabanowitz, J., Hunt, D. F., Neumann, D., and Hart, G. W. (2014) Cross-talk between two essential nutrient-sensitive enzymes: O-GlcNAc transferase (OGT) and AMP-activated protein kinase (AMPK). *J. Biol. Chem. 289*, 10592−10606.

(52) Wani, W. Y., Ouyang, X., Benavides, G. A., Redmann, M., Cofield, S. S., Shacka, J. J., Chatham, J. C., Darley-Usmar, V., and Zhang, J. (2017) O-GlcNAc regulation of autophagy and alpha-synuclein homeostasis; implications for Parkinson's disease. *Mol. Brain 10*, 32.

(53) Andres, L. M., Blong, I. W., Evans, A. C., Rumachik, N. G., Yamaguchi, T., Pham, N. D., Thompson, P., Kohler, J. J., and Bertozzi, C. R. (2017) Chemical Modulation of Protein O-GlcNAcylation via OGT Inhibition Promotes Human Neural Cell Differentiation. *ACS Chem. Biol. 12*, 2030−2039.

(54) Ruan, H. B., Ma, Y., Torres, S., Zhang, B., Feriod, C., Heck, R. M., Qian, K., Fu, M., Li, X., Nathanson, M. H., Bennett, A. M., Nie, Y., Ehrlich, B. E., and Yang, X. (2017) Calcium-dependent O-GlcNAc signaling drives liver autophagy in adaptation to starvation. *Genes Dev. 31*, 1655−1665.

(55) Kumar, A., Singh, P. K., Parihar, R., Dwivedi, V., Lakhotia, S. C., and Ganesh, S. (2014) Decreased O-linked GlcNAcylation protects from cytotoxicity mediated by huntingtin exon1 protein fragment. *J. Biol. Chem. 289*, 13543−13553.

(56) Jo, Y. K., Park, N. Y., Park, S. J., Kim, B. G., Shin, J. H., Jo, D. S., Bae, D. J., Suh, Y. A., Chang, J. H., Lee, E. K., Kim, S. Y., Kim, J. C., and Cho, D. H. (2016) O-GlcNAcylation of ATG4B positively regulates autophagy by increasing its hydroxylase activity. *Oncotarget 7*, 57186−57196.

(57) Adams, B. F., Berry, G. J., Huang, X., Shorthouse, R., Brazelton, T., and Morris, R. E. (2000) Immunosuppressive therapies for the prevention and treatment of obliterative airway disease in heterotopic rat trachea allografts. *Transplantation 69*, 2260−2266.

(58) Lamming, D. W., Ye, L., Katajisto, P., Goncalves, M. D., Saitoh, M., Stevens, D. M., Davis, J. G., Salmon, A. B., Richardson, A., Ahima, R. S., Guertin, D. A., Sabatini, D. M., and Baur, J. A. (2012) Rapamycin-induced insulin resistance is mediated by mTORC2 loss and uncoupled from longevity. *Science 335*, 1638−1643.

(59) Zhang, X., Li, L., Chen, S., Yang, D., Wang, Y., Zhang, X., Wang, Z., and Le, W. (2011) Rapamycin treatment augments motor neuron degeneration in SOD1(G93A) mouse model of amyotrophic lateral sclerosis. *Autophagy 7*, 412−425.

(60) Staats, K. A., Hernandez, S., Schonefeldt, S., Bento-Abreu, A., Dooley, J., Van Damme, P., Liston, A., Robberecht, W., and Van Den Bosch, L. (2013) Rapamycin increases survival in ALS mice lacking mature lymphocytes. *Mol. Neurodegener. 8*, 31.

(61) Grima, J. C., Daigle, J. G., Arbez, N., Cunningham, K. C., Zhang, K., Ochaba, J., Geater, C., Morozko, E., Stocksdale, J., Glatzer, J. C., Pham, J. T., Ahmed, I., Peng, Q., Wadhwa, H., Pletnikova, O., Troncoso, J. C., Duan, W., Snyder, S. H., Ranum, L. P., Thompson, L. M., Lloyd, T. E., Ross, C. A., and Rothstein, J. D. (2017) Mutant Huntingtin Disrupts the Nuclear Pore Complex. *Neuron 94*, 93−107.

(62) Kaech, S., and Banker, G. (2006) Culturing hippocampal neurons. *Nat. Protoc 1*, 2406−2415.

(63) Miranda, C. J., Braun, L., Jiang, Y., Hester, M. E., Zhang, L., Riolo, M., Wang, H., Rao, M., Altura, R. A., and Kaspar, B. K. (2012) Aging brain microenvironment decreases hippocampal neurogenesis through Wnt-mediated survivin signaling. *Aging Cell 11*, 542−552.

(64) Iyirhiaro, G. O., Zhang, Y., Estey, C., O'Hare, M. J., Safarpour, F., Parsanejad, M., Wang, S., Abdel-Messih, E., Callaghan, S. M., During, M. J., Slack, R. S., and Park, D. S. (2014) Regulation of ischemic neuronal death by E2F4-p130 protein complexes. *J. Biol. Chem. 289*, 18202−18213.